# **Energy &** Environmental Science



PAPER

View Article Online



Cite this: Energy Environ. Sci., 2020, 13, 3110

# dominating role of interior modification in surface electrocatalysis†

Boosting alkaline hydrogen evolution: the

Zhao Li, ‡ab Wenhan Niu, (10 ‡b Zhenzhong Yang, (10 ‡c Abdelkader Kara, de Qi Wang, f Maoyu Wang,<sup>9</sup> Meng Gu,\*<sup>f</sup> Zhenxing Feng, (D\*9 Yingge Du\*c and Yang Yang (D\*abe

The alkaline hydrogen evolution reaction (A-HER) holds great promise for clean hydrogen fuel generation but its practical utilization is severely hindered by the sluggish kinetics for water dissociation in alkaline solutions. Traditional ways to improve the electrochemical kinetics for A-HER catalysts have been focusing on surface modification, which still can not meet the demanding requirements for practical water electrolysis because of catalyst surface deactivation. Herein, we report an interior modification strategy to significantly boost the A-HER performance. Specifically, a trace amount of Pt was doped in the interior Co<sub>2</sub>P (Pt-Co<sub>2</sub>P) to introduce a stronger dopant-host interaction than that of the surface-modified catalyst. Consequently, the local chemical state and electronic structure of the catalysts were adjusted to improve the electron mobility and reduce the energy barriers for hydrogen adsorption and H-H bond formation. As a proof-of-concept, the interior-modified Pt-Co<sub>2</sub>P shows a reduced onset potential at near-zero volts for the A-HER, low overpotentials of 2 mV and 58 mV to achieve 10 and 100 mA cm<sup>-2</sup>, and excellent durability for long-term utilization. The interior-modified Pt-Co<sub>2</sub>P delivers superior A-HER performance to Pt/C and other state-of-the-art electrocatalysts. This work will open a new avenue for A-HER catalyst design.

Received 1st June 2020, Accepted 31st July 2020

DOI: 10.1039/d0ee01750g

rsc.li/ees

#### 1. Introduction

Hydrogen gas (H2), as a clean alternative fuel to fossil energy, plays crucial roles in developing a renewable and sustainable energy future due to its zero-carbon-emissions and recyclability. 1-3 Among various H2 generation techniques, water electrolysis is considered as the most efficient process for high-purity H2 production. Especially, the alkaline hydrogen evolution reaction (A-HER) is of great importance for practical water electrolyzers without concerns about contamination from acidic fog and container corrosion involved in the acidic HER.5,6 However, extra energy is always required to break the covalent bonds in water molecules during the A-HER because of the sluggish reaction kinetics for water dissociation. Also, it is very challenging to design catalysts with favorable hydrogen adsorption (hydrogen binding free energy,  $\Delta G_{H^*}$ ) for the A-HER.<sup>8</sup> Thus, it is critical to design more efficient A-HER catalysts that can reduce the energy barrier and facilitate hydrogen adsorption for H-H bond formation in alkaline electrolyte. So far, platinum (Pt)based materials are the dominantly used HER catalysts due to the remarkable electronic conductivity, favorable d-band center relative to the Fermi energy level, and optimized  $\Delta G_{H^*}$ . However, their natural scarcity and high cost restrict their scalable and practical applications. 12,13 It is urgent to design emerging catalysts with high A-HER activity and low Pt loading for water electrolysis.

Transition-metal phosphides (TMPs) such as cobalt phosphide (Co<sub>2</sub>P) have been considered as promising candidates for the HER due to their metalloid property and good electrical conductivity, which offer facilitated catalytic performance in acidic media. 14,15 However, these TMP catalysts suffer from limited HER performance in alkaline solution, owing to the low electron transfer capability and high work function.

<sup>&</sup>lt;sup>a</sup> Department of Materials Science and Engineering, University of Central Florida, Orlando, FL 32826, USA. E-mail: Yang.Yang@ucf.edu

<sup>&</sup>lt;sup>b</sup> NanoScience Technology Center, University of Central Florida, Orlando, FL 32826,

<sup>&</sup>lt;sup>c</sup> Physical and Computational Sciences Directorate, Pacific Northwest National Laboratory, Richland, Washington 99352, USA. E-mail: Yingge.Du@pnnl.gov

<sup>&</sup>lt;sup>d</sup> Department of Physics, University of Central Florida, Orlando, FL 32826, USA

<sup>&</sup>lt;sup>e</sup> Energy Conversion and Propulsion Cluster, University of Central Florida, Orlando, FL 32826, USA

f Department of Materials Science and Engineering, Southern University of Science and Technology, Shenzhen 518055, China. E-mail: gum@sustech.edu.cn

<sup>&</sup>lt;sup>g</sup> School of Chemical, Biological, and Environmental Engineering, Oregon State University, Corvallis, OR 97331, USA. E-mail: zhenxing.feng@oregonstate.edu

<sup>†</sup> Electronic supplementary information (ESI) available: Materials and electrochemical characterizations. See DOI: 10.1039/d0ee01750g

<sup>‡</sup> These authors contributed equally to this work.

Hitherto, the most widely applied strategy to improve the A-HER activities of TMP catalysts is through surface modification. 14,16,17 For instance, Pt nanoparticles, clusters, and atoms have been utilized to modify the catalyst surfaces, achieving improved HER activities by the interactions between the surface Pt and TMP catalysts. 1,8,18,19 However, it is still very difficult to overcome additional energy barriers for adsorbed hydrogen (H\*) migration from Pt to TMP on the catalyst surfaces in alkaline solution. 19-21 Moreover, the electrocatalytic activities of the surface-modified catalysts suffer from deactivation issues because of the surface passivation or surface reconstruction during the A-HER. Thereupon, it is fundamentally interesting and practically meaningful to answer the question: is it possible to boost the A-HER activity by interior modification of catalysts?

Herein, we designed a new strategy that directly answered the aforementioned question by contrasting the A-HER performance of surface-modified Co<sub>2</sub>P (Pt@Co<sub>2</sub>P) with that of the interior-modified Co<sub>2</sub>P counterpart (Pt-Co<sub>2</sub>P) where Pt was kept to the same trace amount ( $\sim$  3.6 wt%). Especially, the impacts of the catalyst modifications on the reaction pathway, ratedetermining step, hydrogen adsorption, and H-H bond formation in alkaline solution were investigated. In contrast to the weak interaction of the surface-modified Pt@Co2P, the strong interaction between the Pt dopant and Co<sub>2</sub>P host in the interiormodified Pt-Co<sub>2</sub>P efficiently adjusts the local chemical state and electronic structure of Pt-Co<sub>2</sub>P, promoting water dissociation, hydrogen adsorption, and H-H bond formation. As a result, Pt-Co<sub>2</sub>P exhibits outstanding A-HER activity with a near-zero onset potential and low overpotentials of 2 mV and 58 mV to reach current densities of 10 mA cm<sup>-2</sup> and 100 mA cm<sup>-2</sup>, which is superior to the commercial Pt/C and other benchmark HER catalysts.<sup>22,23</sup> This work suggests that the interior modification plays a profound role in governing the catalyst performance even though the reactions occur on the surfaces, which may lead to a new paradigm shift from concentrating on surface modification for high-performance HER catalyst design.

### 2. Results and discussion

The fabrication route for the interior-modified Pt-Co<sub>2</sub>P catalyst is illustrated in Fig. 1a (more experimental details in the ESI†). Slightly doped cobalt (Co) by a trace amount of Pt was synthesized by CoPt alloy co-electrodeposition on carbon cloth (CC) followed by thermal phosphorization via chemical vapor deposition (CVD) and surface cleaning via acid. Finally, Pt-Co<sub>2</sub>P particles grown on CC were successfully obtained. The interior-modified Pt-Co<sub>2</sub>P catalyst uniformly grown on CC is binder-free, of high surface area, and tightly in contact with the current collector, endowing the catalyst with greatly reduced charge transfer resistance across the interfaces.<sup>24</sup> By contrast, the surface-modified Pt@Co<sub>2</sub>P was prepared by decorating Co<sub>2</sub>P with electrodeposited Pt nanoparticles. The Pt contents in both the Pt-Co<sub>2</sub>P and Pt@Co<sub>2</sub>P catalysts were measured to be 3.6 wt% by X-ray fluorescence and inductively coupled plasma mass spectroscopy (XRF and ICP-MS, Table S1, ESI†).

The crystal structures of Co<sub>2</sub>P, Pt@Co<sub>2</sub>P, and Pt-Co<sub>2</sub>P were characterized by X-ray diffraction (XRD, Fig. 1b). The characteristic peaks at 40.70°, 43.17°, 50.37°, and 52.01°, marked by asterisks, corresponding to the (121), (211), (310), and (002) planes, respectively, match well with Co<sub>2</sub>P (JCPDS No. 32-0306), indicating the same main crystalline phase of the catalysts. Meanwhile, no diffraction peak of Pt, especially the characteristic peak located at around 39.60° for Pt(111), can be identified in the catalysts, confirming the low content of Pt doping. 13,25,26 The shifted diffraction peaks of Pt-Co<sub>2</sub>P (Fig. S1, ESI†) suggest lattice distortion induced by the incorporation of Pt dopants in the crystal structure of Co<sub>2</sub>P, which contribute to the enhanced catalytic activity. 13

Scanning electron microscopy (SEM) and transmission electron microscopy (TEM) images (Fig. 1c and d) show that Pt-Co<sub>2</sub>P particles with a size distribution from 125 nm to 150 nm uniformly grow on carbon cloth (CC). The high-angle annular dark-field scanning TEM images (HAADF-STEM, Fig. 1e) confirm that a 7-10 nm thin layer was uniformly covered on the surface of Pt-Co<sub>2</sub>P particles. The corresponding energy dispersive spectroscopy (EDS) line scan reveals a higher P-content on the surface of Pt-Co<sub>2</sub>P (Fig. 1f). Catalysts with P-rich surfaces are favorable for enhancing the interaction between the surface active sites and water molecules and thus help to break the H-OH bond.27 The low content of Pt uniformly distributed across Pt-Co<sub>2</sub>P as compared to those of Co and P further confirms the successful incorporation of a trace amount of Pt in the interior Co<sub>2</sub>P. The interior Pt dopants play an important role in modulating the local electronic structure of Co<sub>2</sub>P, which consequently contributes to forming favorable thermo-neutral active sites for the HER. 28 The element composition and distribution of Pt-Co<sub>2</sub>P were analyzed by STEM-EDS mapping (Fig. 1g-j), where Pt and Co were uniformly distributed in the Pt-Co<sub>2</sub>P particles, while higher P concentration was observed on the outmost layer. To further characterize the crystal phase and composition of Pt-Co<sub>2</sub>P particles, the TEM images and the corresponding fast Fourier transformation (FFT) were analyzed in Fig. 1k-o. As shown in the TEM images (Fig. 1k-l), the outmost region can be clearly distinguished from the bulk as marked by the yellow dash lines. Meanwhile, the selected areas 1-4 are indicated by blue and white dash squares in Fig. 1l. The FFT patterns (Fig. 1m) in the blue dash area suggest that the outmost regions have two sets of lattice spacings (1.78 Å and 2.03 Å; and 2.18 Å and 2.02 Å), corresponding to the (311) and (310); and (121) and (310) facets of Co<sub>2</sub>P, respectively. The high-resolution TEM (HRTEM) images in Fig. 1n further reveal the disordered lattice structures observed in the outmost region, suggesting imperfect crystallization caused by defects formed in the P-rich surface layer.<sup>2</sup> The interior Pt-Co<sub>2</sub>P identified by the FFT pattern (Fig. 1m) shows that the lattice spacings (3.20 Å and 1.79 Å) belonging to the (101) and (002) facets of Co<sub>2</sub>P slightly increased as compared to the standard Co<sub>2</sub>P because of the Pt doping effect. Meanwhile, the atomic-resolution images illustrated in Fig. S2 (ESI†) reveal no obvious Pt clusters grown in Pt-Co<sub>2</sub>P. All the above evidence strongly proves that Pt has been uniformly

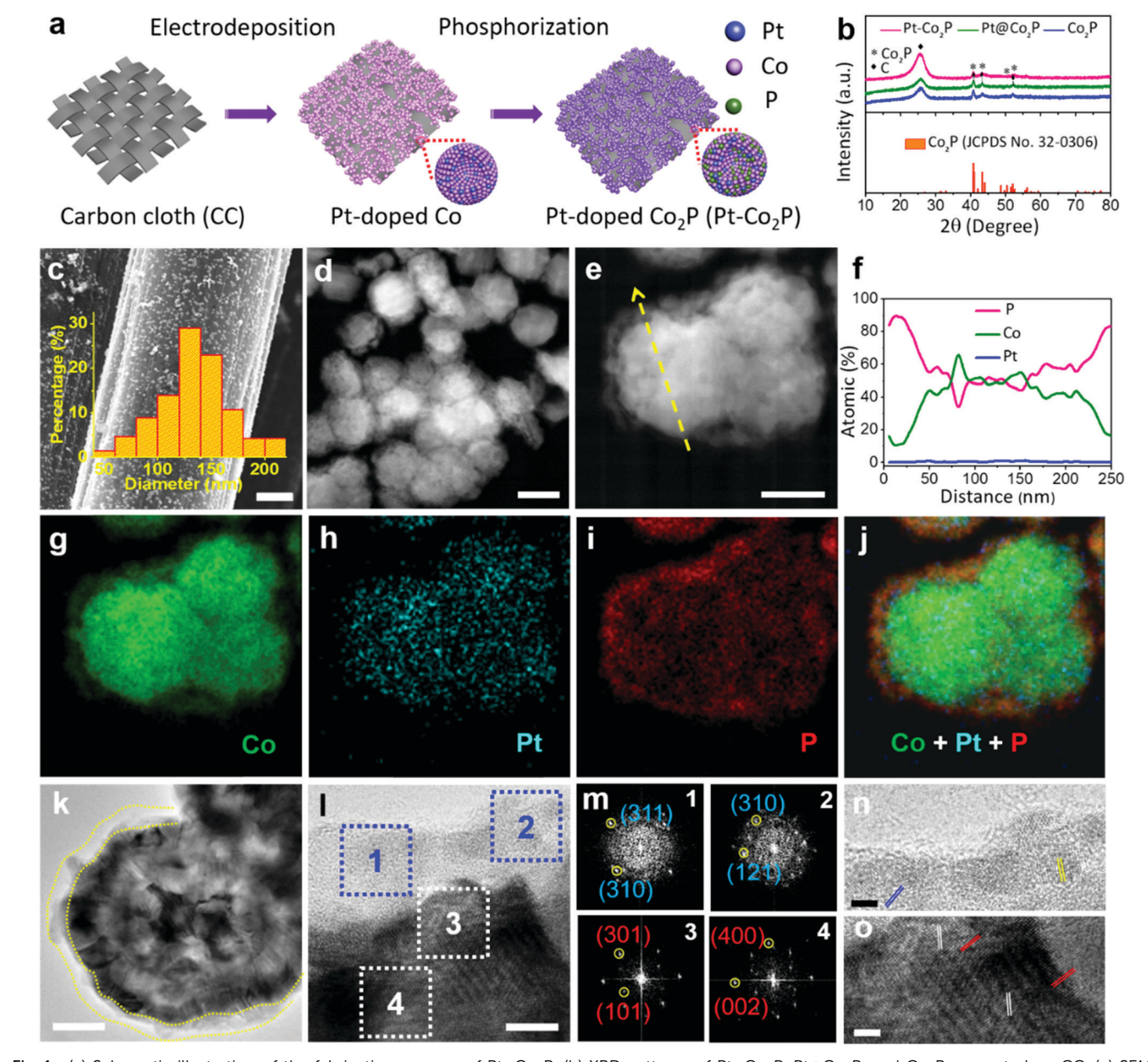


Fig. 1 (a) Schematic illustration of the fabrication process of Pt-Co<sub>2</sub>P. (b) XRD patterns of Pt-Co<sub>2</sub>P, Pt@Co<sub>2</sub>P, and Co<sub>2</sub>P supported on CC. (c) SEM images of Pt-Co<sub>2</sub>P particles grown on CC. The inset is the particle size distribution. Scale bar: 2 μm. (d and e) HAADF-STEM images of Pt-Co<sub>2</sub>P. Scale bars: 200 nm and 100 nm, respectively. (f-j) EDS line scan and STEM-EDS elemental mapping. (k and l) High-resolution TEM images of Pt-Co<sub>2</sub>P. Scale bars: 50 nm and 5 nm, respectively. (m) FFT patterns selected from the blue and white dash zones in (l), where zones 1-2 and 3-4 represent the P-rich surface and well-crystallized interior Co<sub>2</sub>P, respectively. (n and o) Lattice spacings of Pt-Co<sub>2</sub>P. Scale bar: 2 nm. Note that the blue, yellow, red, and white lines represent the Co<sub>2</sub>P (311), (121), (301), and (002) planes, respectively.

doped into our Pt-Co<sub>2</sub>P catalyst. In addition, Pt@Co<sub>2</sub>P was also characterized as shown in Fig. S3 (ESI†). Different from Pt-Co<sub>2</sub>P, the TEM image of Pt@Co<sub>2</sub>P (Fig. S3a and b, ESI†) shows that Pt nanoparticles (~5 nm) uniformly anchor on the surface of Co<sub>2</sub>P. The EDS element mapping confirms the coexistence of Co, P, and Pt in Pt@Co2P with concentrated Pt in the outmost layer, further verifying that Pt nanoparticles are decorated on the surface of Co<sub>2</sub>P (Fig. S3c-f, ESI†).

X-ray photoelectron spectroscopy (XPS) and X-ray absorption spectroscopy (XAS) including the X-ray absorption near-edge

structure (XANES) and extended X-ray absorption fine structure (EXAFS) were employed to study the impacts of the catalyst (surface or interior) modification methods on the chemical states, local bonding, electronic structures, and compositions of Pt-Co<sub>2</sub>P, Pt@Co<sub>2</sub>P, and Co<sub>2</sub>P. The high-resolution XPS spectra confirm the existence of Pt, Co, and P in the catalysts (Fig. 2a-c). The XPS Pt peaks (Fig. 2a) for Pt-Co<sub>2</sub>P located at 71.12 eV and 74.44 eV are assigned to metallic Pt(0). The two XPS peaks at 72.33 eV and 75.61 eV are ascribed to  $4f_{7/2}$  and 4f<sub>5/2</sub> of Pt(2+).<sup>29</sup> It also suggests that Pt-Co<sub>2</sub>P has a higher

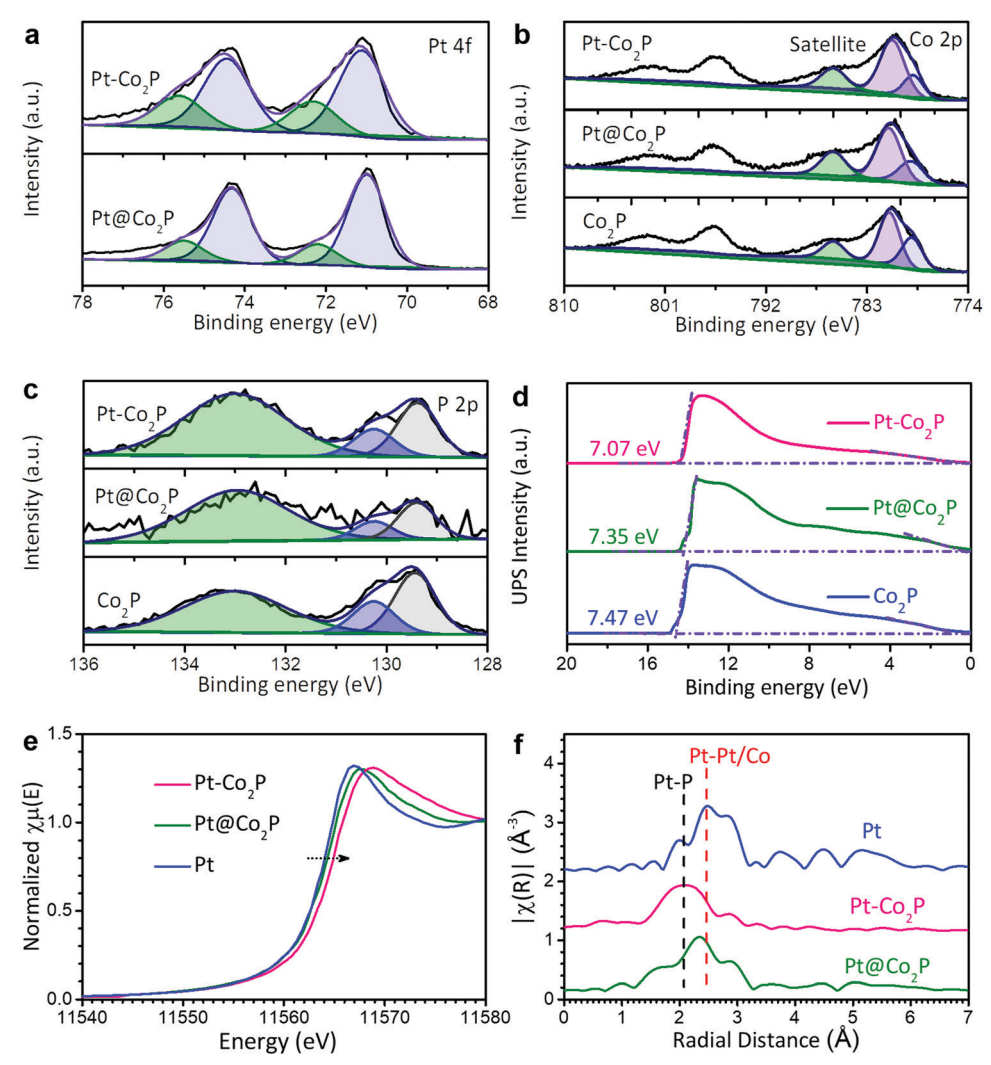


Fig. 2 Spectral investigation of the catalysts by XPS and UPS. The high-resolution XPS spectra of (a) Pt 4f, (b) Co 2p, and (c) P 2p. (d) UPS spectra of the catalysts. The Pt L-edge (e) XANES, and (f) EXAFS spectra of Pt, Pt-Co<sub>2</sub>P, and Pt@Co<sub>2</sub>P, respectively

atomic ratio of Pt<sup>2+</sup>/Pt<sup>0</sup> (0.4, Table S2, ESI†) than that of Pt@Co<sub>2</sub>P (0.24), indicating a stronger electronic interaction between Pt atoms and Co<sub>2</sub>P for regulating hydrogen evolution.<sup>30</sup> The highresolution XPS Co 2p<sub>3/2</sub> peaks (Fig. 2b) for Pt-Co<sub>2</sub>P located at 778.79 eV and 780.91 eV are assigned to the Co-P bond in Co<sub>2</sub>P.<sup>31</sup> Furthermore, the Co<sup>2+</sup>/Co<sup>3+</sup> ratio estimated by fitting the XPS Co 2p<sub>3/2</sub> peaks for Pt-Co<sub>2</sub>P is higher than that for Pt@Co<sub>2</sub>P (Table S3, ESI†), further confirming a stronger electronic interaction in the interior-modified Pt-Co<sub>2</sub>P than the surfacemodified Pt@Co<sub>2</sub>P.32-34 The high-resolution XPS P 2p peaks (Fig. 2c) located at 129.45 eV and 130.28 eV correspond to P 2p<sub>3/2</sub> and P  $2p_{1/2}$  for the negatively charged P (Co-P bond) in  $Co_2P$ . <sup>35,36</sup> An isolated peak at 133.14 eV indicates the naturally oxidized P on the catalyst surface, which has been reported in many TMP catalysts. 37-39

Ultraviolet photoelectron spectroscopy (UPS, Fig. 2d) was used to explore the impacts of the modification methods (Pt on the surface or in the interior of Co<sub>2</sub>P) on the energy levels of Pt-Co<sub>2</sub>P, Pt@Co<sub>2</sub>P, and Co<sub>2</sub>P, which were estimated to be 7.07 eV, 7.35 eV, and 7.47 eV, respectively, by subtracting 21.22 eV

of He I UPS spectra. The lower energy level of Pt-Co2P indicates higher electron mobility for hydrogen generation than Pt@Co2P and Co<sub>2</sub>P. 40 Moreover, the Pt dopants in the Pt-Co<sub>2</sub>P catalyst can modulate the local electronic structure and the chemical state of  $Co_2P$ , thus resulting in considerable active sites and delicate  $\Delta G_{H^*}$ for an efficient A-HER.

To understand the oxidation state and corresponding local structure of our catalysts, XAS, 41-43 including XANES and EXAFS, was performed and is shown in Fig. 2e and f. The corresponding XANES edge of Pt-Co<sub>2</sub>P shifts to higher energy compared to Pt@Co2P and Pt. It suggests a higher oxidation state of Pt in Pt-Co<sub>2</sub>P, agreeing well with the results from XPS analysis. For EXAFS, the peak around 2.1 Å in Pt-Co<sub>2</sub>P is shorter than the Pt-Pt metal peak (2.5 Å) in Pt metal, which could be treated as a Pt-P peak or Pt-Co peak. To further verify the local coordination structure of Pt, we used the structure model generated from theoretical calculations to fit the EXAFS spectrum of Pt-Co<sub>2</sub>P. The analysis (Fig. S4 and Table S4, ESI†) shows the co-existence of Pt-P and Pt-Co bonds, which

confirms that Pt doped into the  $Co_2P$  matrix with P. The higher amplitude of Pt–P and Pt–Co in the EXAFS of Pt– $Co_2P$  than that of Pt@ $Co_2P$  also indicates the stronger dopant–host interaction in Pt– $Co_2P$ . Consequently, the local electronic structure of Pt– $Co_2P$  can be effectively modified by the regulation of the energy levels as illustrated in UPS (Fig. 2d). It is favorable for the enhancement of electron mobility and reducing the energy barriers for the A-HER with high efficiency.

To further study the structure-property relationship of the catalysts, the A-HER performance of Pt-Co<sub>2</sub>P, Pt@Co<sub>2</sub>P, and

control samples such as  $Co_2P$  and Pt/C was examined in a typical three-electrode cell in alkaline solution (Fig. 3a–c). All the polarization curves were treated with iR-compensation. The reference electrode was calibrated in a high purity  $H_2$ -saturated electrolyte (Fig. S5, ESI†). Linear sweep voltammetry (LSV) curves (Fig. 1a and Fig. S6, ESI†) show that  $Co_2P$  exhibits an inferior A-HER performance (*e.g.* larger overpotentials at different current densities) among all the catalysts. Both surface-modified  $Pt@Co_2P$  and interior-modified  $Pt-Co_2P$  show significantly improved A-HER performance by introducing a

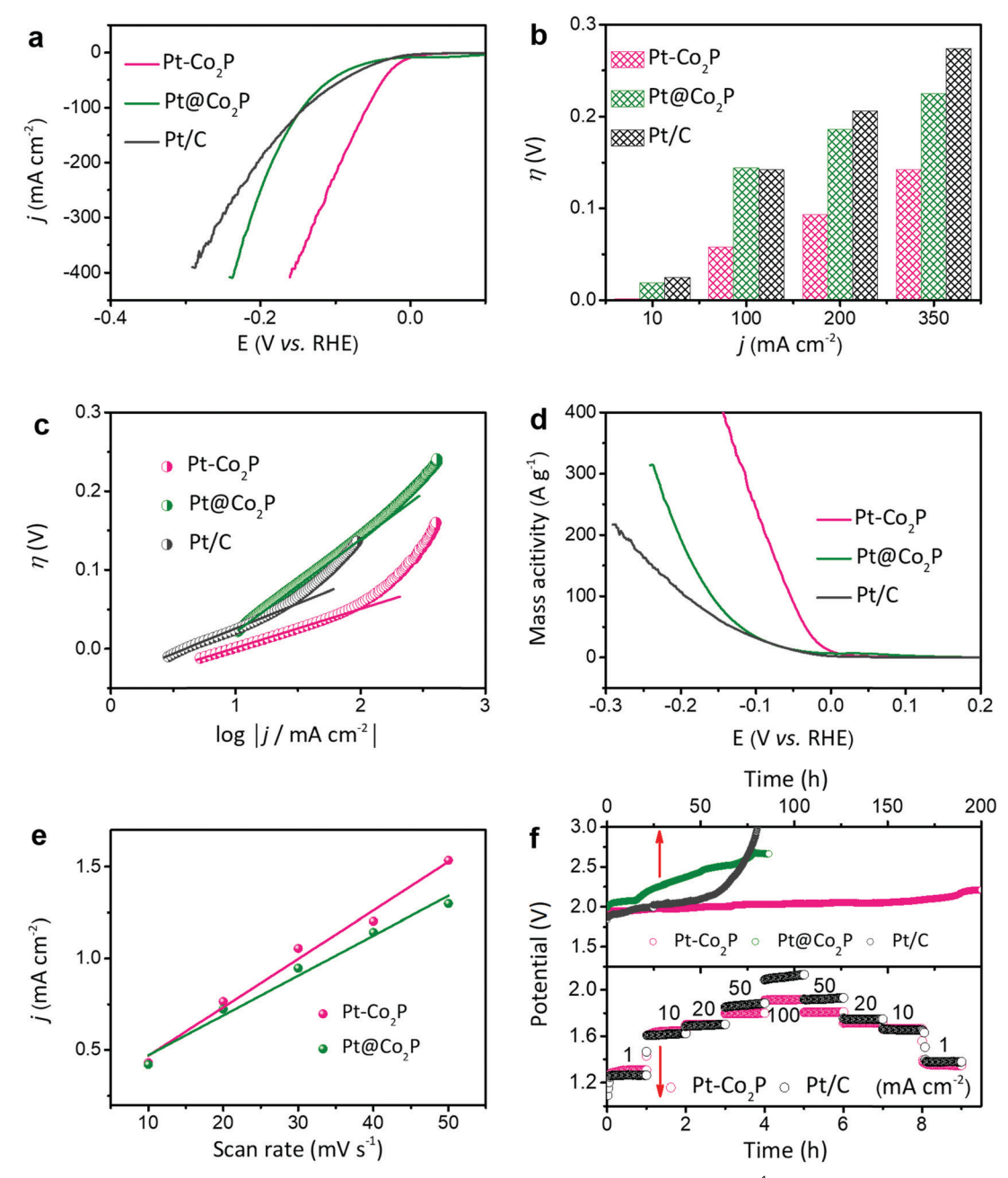


Fig. 3 A-HER performance of the catalysts in 1 M KOH. (a) LSV curves of the catalysts tested at 5 mV s $^{-1}$ . (b) The overpotentials required to achieve different current densities (10, 100, 200, and 350 mA cm $^{-2}$ ). (c) Tafel plots. (d) Mass activities at different overpotentials. (e) The ECSA of Pt $^{-1}$ Co $^{-1}$ P and Pt $^{-1}$ Co $^{-1}$ P. (f) The stability at 100 mA cm $^{-2}$  and overall water splitting performance of the catalysts at different current densities (1, 10, 20, 50, and 100 mA cm $^{-2}$ ) in a two-electrode set-up with a carbon rod as the counter electrode.

trace amount of Pt into Co<sub>2</sub>P. Especially, Pt-Co<sub>2</sub>P delivers a much lower overpotential of 2 mV to achieve 10 mA cm<sup>-2</sup> than those of Pt@Co2P (19 mV), commercial Pt/C (20 mV), and the state-of-the-art HER catalysts (Table S5, ESI†). It should be noted that the overpotentials of Pt-Co<sub>2</sub>P are still prominently lower than those of Pt@Co2P and Pt/C at increased current densities, indicating improved H2 bubble release and favorable reactant adsorption. 44 We also tested the repeatability of Pt-Co<sub>2</sub>P for the A-HER (Fig. S7, ESI†) using three Pt-Co<sub>2</sub>P catalysts fabricated from different batches, showing almost consistent A-HER activities and the excellent reproducibility of Pt-Co<sub>2</sub>P. The electrocatalytic A-HER performance tested by LSV directly validates our hypothesis that the interior-modified Pt-Co<sub>2</sub>P prepared by introducing Pt species into the interior Co<sub>2</sub>P could efficiently improve the A-HER activity of Co<sub>2</sub>P as compared to the surface-modified Pt@Co<sub>2</sub>P and Pt/C. The PtCo alloy (Fig. S8-S10, ESI†) was further examined to verify the interior modification as a general approach in regulating the A-HER performance. Moreover, the Tafel slopes were analyzed to have insights into the reaction kinetics for the A-HER. The Tafel slope (Fig. 3c) for Pt@Co<sub>2</sub>P was estimated to be 119 mV dec<sup>-1</sup>, indicating that the A-HER is dominated by the Volmer step due to the sluggish kinetics for water dissociation. 40 However, Pt-Co2P shows a much smaller Tafel slope of 44 mV dec<sup>-1</sup> than those of Pt@Co<sub>2</sub>P and commercial Pt/C (65 mV dec<sup>-1</sup>), suggesting a favorable Volmer-Heyrovsky pathway and facilitated electron transfer kinetics for the A-HER.

The mass activity and electrochemically active surface area (ECSA) were also evaluated to provide an insightful understanding of the intrinsic activities of the catalysts. As shown in Fig. 3d, Pt-Co<sub>2</sub>P delivers a higher mass activity than Pt@Co<sub>2</sub>P and Pt/C at different overpotentials, strongly supporting our hypothesis that the interior modification of Co<sub>2</sub>P is more efficient than the traditional surface modification. 45 Furthermore, the ECSA was estimated by calculating the double-layer capacitance ( $C_{\rm dl}$ , Fig. 3e).  $^{46,47}$   $C_{\rm dl}$  of Pt-Co<sub>2</sub>P (26.48 mF cm<sup>-2</sup>) is higher than those of Pt@Co<sub>2</sub>P (21.77 mF cm<sup>-2</sup>) and Co<sub>2</sub>P (13.38 mF cm<sup>-2</sup>, Fig. S11, ESI†), indicating that the Pt doping in the interior Co<sub>2</sub>P increases the ECSA and overall active sites. It is further direct evidence proving our concept that the Pt dopants incorporated in the interior Co<sub>2</sub>P strongly interact with surrounding Co and P, leading to greatly increased surface active sites for the A-HER.

To further understand the drastically improved A-HER performance of Pt-Co<sub>2</sub>P through the interior Pt doping, more solid pieces of evidence are demonstrated in Fig. S12-S15 (ESI†). First of all, the underpotential deposition (UPD) method was adopted to evaluate the density of active sites. 48 The CV curves of Pt-Co<sub>2</sub>P and Pt@Co<sub>2</sub>P in Fig. S12 (ESI†) demonstrate the signal of underpotential Cu stripping corresponding to the number of active sites for the catalytic reactions. The stronger intensity of the underpotential Cu stripping for Pt-Co<sub>2</sub>P indicates an increased number of active sites when compared with that for Pt@Co<sub>2</sub>P.<sup>3,49</sup> Precisely, the density of the active sites was calculated to be  $1.02 \times 10^{18}$  sites per cm<sup>2</sup> for Pt-Co<sub>2</sub>P, greater than that of Pt@Co<sub>2</sub>P (7.45  $\times$  10<sup>17</sup> sites per cm<sup>2</sup>, Fig. S13, ESI†). Besides, the turnover frequency (TOF) for Pt-Co<sub>2</sub>P is greater than that of Pt@Co<sub>2</sub>P at the same overpotential (Fig. S14, ESI†). To build a relationship of the Tafel plots with the TOF, the exchange current measured from Fig. 3c was further employed to evaluate the value of the TOF for Pt-Co<sub>2</sub>P as 0.031 s<sup>-1</sup>, outperforming that of Pt@Co<sub>2</sub>P (0.026 s<sup>-1</sup>).<sup>50</sup> Furthermore, to evaluate the intrinsic activity of our catalysts, the quantitative characterizations of the electrocatalytic activities, including the LSV curves, Tafel slope, mass activity, and TOF, were normalized by the ECSA (Fig. S15, ESI†). The electrochemical activities of Pt-Co<sub>2</sub>P are superior to Pt@Co<sub>2</sub>P, proving its remarkably intrinsic activity. To validate the importance of the interior Pt dopant in Pt-Co<sub>2</sub>P, a full range of CV curves were recorded as shown in Fig. S16 (ESI†). No characteristic Pt-based H/OH adsorption and desorption peaks can be detected from Pt-Co<sub>2</sub>P in alkaline and acid electrolyte. It reveals that Pt in Pt-Co<sub>2</sub>P is not the primarily exposed surface active site. From another perspective, it indirectly highlights the significance of incorporation of the interior Pt dopant in the regulation of the electronic structure of Co<sub>2</sub>P and consequently the promotion of the overall catalytic performance of Pt-Co<sub>2</sub>P.

The A-HER stabilities for the catalysts were galvanostatically examined in a two-electrode set-up with a carbon rod as the counter electrode in 1 M KOH for overall water splitting (Fig. 3f). Pt-Co<sub>2</sub>P can keep the potential at a current density of 100 mA cm<sup>-2</sup> for 200 hours. However, unfortunately, Pt@Co<sub>2</sub>P and Pt/C show poor stabilities during the long-term testing, which is mainly due to catalyst deactivation in extreme alkaline solution. In addition, we also examined the galvanostatic stabilities of Pt-Co<sub>2</sub>P as compared to commercial Pt/C at different current densities from 1 mA cm<sup>-2</sup> to 100 mA cm<sup>-2</sup>. With increasing the current density, the required potential for overall water splitting increases gradually. Meanwhile, Pt-Co<sub>2</sub>P exhibits better reversibility and durability than Pt/C when decreasing the current density. Furthermore, to verify our catalyst as a favorite electrode during long stability tests, both high-resolution TEM images and EXAFS of the Pt L-edge corresponding to Pt-Co2P were recorded after the stability test as shown in Fig. S17 and S18 (ESI†). It gives close results to those before the stability test, suggesting almost negligible structural changes. Moreover, with model-based analysis (Table S6, ESI†), we could not find any change in coordination number for all related Pt-P and Pt-Co bonds, suggesting the robustness of Pt-Co<sub>2</sub>P realized by interior modification.

Moreover, density functional theory (DFT) calculations were used to understand the catalytic mechanism of Pt-Co<sub>2</sub>P (more calculation details in the ESI†). The atomic structure models were built up with and without the incorporation of the Pt dopant, whose presence could alter the local atomic and electronic structure of Co<sub>2</sub>P. Firstly, the partial densities of states (PDOS, Fig. 4a) were evaluated to understand the role of Pt doping in the improved intrinsic A-HER activity. The calculation results suggest that the Pt dopant can greatly impact the electronic states of Pt-Co<sub>2</sub>P, consistent with XPS and UPS results. Specifically, the PDOS near the Fermi level is greatly enhanced as a result of the dopant-host interaction.<sup>51</sup> Note that the efficient changes in the Co PDOS reveal its dominant role in

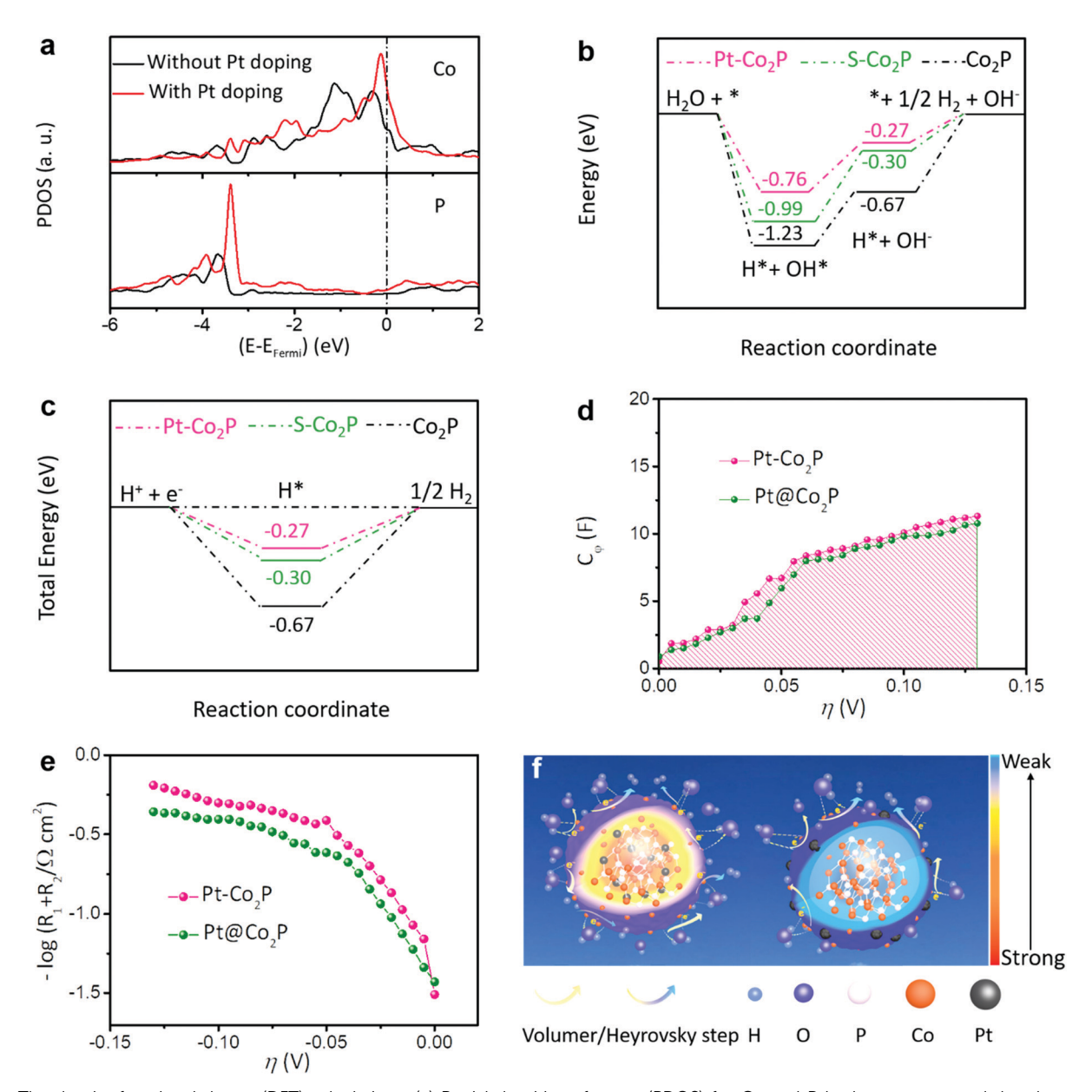


Fig. 4 The density functional theory (DFT) calculations. (a) Partial densities of states (PDOS) for Co and P in the presence and the absence of Pt doping. (b) DFT calculated reaction pathway and (c) calculated H adsorption energies for Pt-Co<sub>2</sub>P, S-Co<sub>2</sub>P, and Co<sub>2</sub>P, respectively. (d) The  $C_{\varphi}$ - $\eta$  plot for Pt-Co<sub>2</sub>P and Pt@Co<sub>2</sub>P. (e) The EIS-Tafel plots. (f) The proposed A-HER mechanism and reaction pathways for Pt-Co<sub>2</sub>P (left) and Pt@Co<sub>2</sub>P (right). The charge intensity is suggested by the color scale bar. The balls with red, white, black, purple, and transparent colors represent Co, P, Pt, O, and H atoms, respectively.

the enhanced catalytic activity. Moreover, DFT calculations were further employed to understand how the components inside Pt-Co<sub>2</sub>P cooperate synergistically to activate the A-HER. It is worth highlighting that we replaced 8 (out of 16) Co surface atoms with P atoms, reaching a 50/50 stoichiometry to mimic the surface P-rich Co<sub>2</sub>P (denoted as S-Co<sub>2</sub>P), trying to correlate well with the results from STEM-EDS and XPS (Fig. 1e, f and 2b, c). Fig. 4b shows the energy diagrams of the A-HER for Pt-Co<sub>2</sub>P, S-Co<sub>2</sub>P, and Co<sub>2</sub>P. In comparison with Co<sub>2</sub>P, the lower energy barriers for Pt-Co<sub>2</sub>P and S-Co<sub>2</sub>P confirm the role of phosphor in accelerating water dissociation. Moreover, the adsorption of H and OH was calculated at different adsorption sites. We found that H and OH prefer binding to Co atoms, revealing Co atoms as the main active sites for the A-HER. Overall, the difference in total energy between the case where both H and OH are adsorbed on the surface and the case where H is adsorbed and OH released from the surface of Pt-Co<sub>2</sub>P is lowest (0.49 eV). Furthermore, the energy as shown in Fig. 4c suggests a preferred A-HER for Pt-Co<sub>2</sub>P as compared to S-Co<sub>2</sub>P and Co<sub>2</sub>P. All the above evidence proves that the Pt dopant can regulate the hydrogen adsorption and H-H bond formation for an enhanced A-HER following the Volmer-Heyrovsky mechanism.

Electrochemical impedance spectroscopy (EIS) was further carried out to explore the charge transfer kinetics for the

electrochemical processes involved in the A-HER, including hydrogen adsorption and H-H bond formation.<sup>52</sup> As shown in Fig. S19 (ESI $\dagger$ ), a smaller charge transfer resistance ( $R_1$ ) for Pt-Co<sub>2</sub>P than Pt@Co<sub>2</sub>P was observed, suggesting enhanced electronic conductivity and accelerated reaction kinetics. Note that the hydrogen adsorption resistance  $(R_2)$  and the corresponding pseudo-capacitances  $(C_{\varphi})$  can be estimated by EIS. As demonstrated in Fig. S20 and S21 (ESI†), R2 for Pt-Co2P is overpotential-dependent and smaller than that for Pt@Co<sub>2</sub>P, revealing improved hydrogen adsorption resulting from the strong electronic interaction between the Pt dopant and Co<sub>2</sub>P host. Furthermore, the hydrogen coverage estimated by  $C_{\omega}$  as a function of the overpotential (Fig. 4d) was used as indirect evidence for hydrogen adsorption on the catalyst surface. The integral area of Pt-Co<sub>2</sub>P (hydrogen adsorption charge) is larger than that of Pt@Co<sub>2</sub>P, suggesting increased hydrogen adsorption as a result of the favorable water dissociation. As shown in the EIS-Tafel plots (Fig. 4e), Pt-Co<sub>2</sub>P shows higher activity than Pt@Co<sub>2</sub>P, further confirming the regulated hydrogen adsorption and H-H bond formation for the enhanced A-HER.<sup>52</sup>

A possible mechanism for the improved A-HER activity of Co<sub>2</sub>P by interior modification using a trace amount of Pt is illustrated in Fig. 4f. The overall A-HER process for both Pt-Co<sub>2</sub>P and Pt@Co<sub>2</sub>P follows the Volmer-Heyrovsky pathway; however, they are dominated by different rate-determining steps. For Pt-Co<sub>2</sub>P (left schematic in Fig. 4f), the Pt doping in the interior Co<sub>2</sub>P can optimize the electronic structure of the catalyst. The P-rich surface is favorable for water dissociation as explained by the DFT calculations (Fig. 4b). Because of the modified electronic structure, H\* could be easily formed and converted to H2 through the Heyrovsky step on the active Co sites, which is the rate-determining step for Pt-Co<sub>2</sub>P. Whereas the rate-determining step for the surface-modified Pt@Co2P (right schematic in Fig. 4f) is dominated by the Volmer step due to the insufficiently optimized local electronic structure.

A series of catalysts, including Pt-Ni<sub>2,25</sub>P, Pt-ZnP<sub>4</sub>, and Pt-WP, were synthesized using the proposed interior-modification strategy (Fig. S22, ESI†) to further verify the versatility of the technique. In comparison with our Pt-Co<sub>2</sub>P, they possess distinguished HER performance as well, proving that our design conception can be considered as a universal strategy in designing novel catalysts.

#### 3. Conclusion

In summary, a new strategy for modulating the local electronic structure of the catalyst for the A-HER by interior modification was designed. The interior-modified Pt-Co<sub>2</sub>P provides an adjusted electronic structure, which is favorable for water dissociation and hydrogen evolution. Specifically, the Pt doping in the interior Co<sub>2</sub>P reduces the energy barriers for hydrogen adsorption and H-H bond formation. As a proof-of-concept, Pt-Co<sub>2</sub>P possesses a near-zero onset potential for the A-HER and lower overpotentials of 5 mV and 58 mV to achieve 10 mA cm<sup>-2</sup> and 100 mA cm<sup>-2</sup>, respectively. Besides, the unique Pt-Co<sub>2</sub>P

catalyst with excellent electrochemical durability and reversibility is favorable for overall water splitting. This work provides a new paradigm for the rational design of efficient catalysts for the A-HER.

#### Conflicts of interest

There are no conflicts to declare.

## Acknowledgements

This work was supported by the National Science Foundation under Grant No. CMMI-1851674 and the startup grant from the University of Central Florida. The XPS test was supported by the NSF MRI XPS: ECCS: 1726636, hosted in the MCF-AMPAC facility, MSE, CECS, UCF. TEM and data analysis were supported by the U.S. Department of Energy, Office of Science, Office of Basic Energy Sciences, Early Career Research Program under award # 68278. A portion of the research was performed using EMSL, a DOE User Facility sponsored by the Office of Biological and Environmental Research and located at the Pacific Northwest National Laboratory. Part of the microscopy work of MG was supported by the National Natural Science Foundation of China (No. 21802065). The computational work of AK is supported by the U.S. Department of Energy Basic Energy Science under Contract No DE-FG02-11ER16243. Resources of the National Energy Research Scientific Computing Center (NERSC) were used for the computational part of this paper. This research used resources of the beamline 5-BM-D, of DND-CAT at the Advanced Photon Source (APS), a U.S. Department of Energy (DOE) Office of Science User Facility operated for the DOE Office of Science by Argonne National Laboratory under Contract DE-AC02-06CH11357. DND-CAT is supported through E. I. duPont de Nemours & Co., Northwestern University, and The Dow Chemical Company.

#### References

- 1 H. Zhang, P. An, W. Zhou, B. Y. Guan, P. Zhang, J. Dong and X. W. D. Lou, Sci. Adv., 2018, 4, eaao6657.
- 2 Z. Li, W. Niu, L. Zhou and Y. Yang, ACS Energy Lett., 2018, 3,
- 3 X. Zhang, Z. Luo, P. Yu, Y. Cai, Y. Du, D. Wu, S. Gao, C. Tan, Z. Li, M. Ren, T. Osipowicz, S. Chen, Z. Jiang, J. Li, Y. Huang, J. Yang, Y. Chen, C. Y. Ang, Y. Zhao, P. Wang, L. Song, X. Wu, Z. Liu, A. Borgna and H. Zhang, Nat. Catal., 2018, 1,
- 4 X. Zou and Y. Zhang, Chem. Soc. Rev., 2015, 44, 5148-5180.
- 5 N. Mahmood, Y. Yao, J. W. Zhang, L. Pan, X. Zhang and J. J. Zou, Adv. Sci., 2018, 5, 1700464.
- 6 Z. F. Huang, J. Song, K. Li, M. Tahir, Y. T. Wang, L. Pan, L. Wang, X. Zhang and J. J. Zou, J. Am. Chem. Soc., 2016, 138, 1359-1365.
- 7 J. X. Feng, J. Q. Wu, Y. X. Tong and G. R. Li, J. Am. Chem. Soc., 2018, 140, 610-617.

- 8 J. Park, S. Lee, H.-E. Kim, A. Cho, S. Kim, Y. Ye, J. W. Han, H. Lee, J. H. Jang and J. Lee, *Angew. Chem., Int. Ed.*, 2019, 131, 16184–16188.
- 9 Z. W. Seh, J. Kibsgaard, C. F. Dickens, I. Chorkendorff, J. K. Norskov and T. F. Jaramillo, *Science*, 2017, 355, eaad4998.
- B. Chen, G. Sun, J. Wang, G. Liu, C. Tan, Y. Chen, H. Cheng,
  J. Chen, Q. Ma and L. Huang, *Chem. Commun.*, 2020, 56,
  5131–5134.
- 11 Z. Zhang, G. Liu, X. Cui, B. Chen, Y. Zhu, Y. Gong, F. Saleem, S. Xi, Y. Du and A. Borgna, *Adv. Mater.*, 2018, 30, 1801741.
- 12 G. Wang, Z. Yang, Y. Du and Y. Yang, *Angew. Chem., Int. Ed.*, 2019, **131**, 15995–16001.
- 13 Z. Li, W. Niu, Z. Yang, N. Zaman, W. Samarakoon, M. Wang, A. Kara, M. Lucero, M. V. Vyas and H. Cao, *Energy Environ. Sci.*, 2020, 13, 884–895.
- 14 C. Tang, L. Gan, R. Zhang, W. Lu, X. Jiang, A. M. Asiri, X. Sun, J. Wang and L. Chen, *Nano Lett.*, 2016, 16, 6617–6621.
- 15 J. Tian, Q. Liu, N. Cheng, A. M. Asiri and X. Sun, *Angew. Chem., Int. Ed.*, 2014, 53, 9577–9581.
- 16 K. Xu, H. Cheng, H. Lv, J. Wang, L. Liu, S. Liu, X. Wu, W. Chu, C. Wu and Y. Xie, Adv. Mater., 2018, 30, 1703344.
- 17 K. Xu, H. Ding, M. Zhang, M. Chen, Z. Hao, L. Zhang, C. Wu and Y. Xie, *Adv. Mater.*, 2017, **29**, 1606980.
- 18 Z. Wang, X. Ren, Y. Luo, L. Wang, G. Cui, F. Xie, H. Wang, Y. Xie and X. Sun, *Nanoscale*, 2018, 10, 12302–12307.
- 19 J. Li, H.-X. Liu, W. Gou, M. Zhang, Z. Xia, S. Zhang, C.-R. Chang, Y. Ma and Y. Qu, Energy Environ. Sci., 2019, 12, 2298–2304.
- 20 C. Tang, R. Zhang, W. Lu, L. He, X. Jiang, A. M. Asiri and X. Sun, *Adv. Mater.*, 2017, **29**, 1602441.
- 21 M. Choi, S. Yook and H. Kim, *ChemCatChem*, 2015, 7, 1048–1057.
- 22 P. Xiao, W. Chen and X. Wang, Adv. Energy Mater., 2015, 5, 1500985.
- 23 G. Zhao, K. Rui, S. X. Dou and W. Sun, Adv. Funct. Mater., 2018, 28, 1803291.
- 24 K. Liang, L. Li and Y. Yang, ACS Energy Lett., 2017, 2, 373-390.
- 25 J. Jones, H. Xiong, A. T. DeLaRiva, E. J. Peterson, H. Pham, S. R. Challa, G. Qi, S. Oh, M. H. Wiebenga and X. I. P. Hernández, *Science*, 2016, 353, 150–154.
- 26 M. A. Shah, Sci. Iran., 2012, 19, 964-966.
- 27 R. Zhang, X. Wang, S. Yu, T. Wen, X. Zhu, F. Yang, X. Sun, X. Wang and W. Hu, *Adv. Mater.*, 2017, **29**, 1605502.
- 28 M. Lao, K. Rui, G. Zhao, P. Cui, X. Zheng, S. X. Dou and W. Sun, *Angew. Chem., Int. Ed.*, 2019, **58**, 5432–5437.
- 29 J. Zhu, G. He and P. K. Shen, *J. Power Sources*, 2015, 275, 279–283.
- 30 M. Lao, K. Rui, G. Zhao, P. Cui, X. Zheng, S. X. Dou and W. Sun, *Angew. Chem., Int. Ed.*, 2019, **58**, 5432–5437.
- 31 A. Dutta, A. K. Samantara, S. K. Dutta, B. K. Jena and N. Pradhan, *ACS Energy Lett.*, 2016, **1**, 169–174.

- 32 S. A. Makhlouf, M. A. Kassem and M. A. Abdel-Rahim, J. Mater. Sci., 2009, 44, 3438-3444.
- 33 J. Zhang, X. Wu, W. C. Cheong, W. Chen, R. Lin, J. Li, L. Zheng, W. Yan, L. Gu, C. Chen, Q. Peng, D. Wang and Y. Li, *Nat. Commun.*, 2018, 9, 1002.
- 34 H. Wu, G. Wu, Y. Ren, L. Yang, L. Wang and X. Li, *J. Mater. Chem. C*, 2015, 3, 7677–7690.
- 35 J. Song, C. Zhu, B. Z. Xu, S. Fu, M. H. Engelhard, R. Ye, D. Du, S. P. Beckman and Y. Lin, *Adv. Energy Mater.*, 2017, 7, 1601555.
- 36 Z. Huang, Z. Chen, Z. Chen, C. Lv, M. G. Humphrey and C. Zhang, *Nano Energy*, 2014, 9, 373–382.
- 37 Q. Gao, W. Zhang, Z. Shi, L. Yang and Y. Tang, *Adv. Mater.*, 2019, 31, e1802880.
- 38 K. Liang, S. Pakhira, Z. Yang, A. Nijamudheen, L. Ju, M. Wang, C. I. Aguirre-Velez, G. E. Sterbinsky, Y. Du, Z. Feng, J. L. Mendoza-Cortes and Y. Yang, ACS Catal., 2019, 9, 651–659.
- 39 Y. Yang, H. Fei, G. Ruan and J. M. Tour, *Adv. Mater.*, 2015, 27, 3175–3180.
- 40 Y. Shi, Y. Zhou, D. R. Yang, W. X. Xu, C. Wang, F. B. Wang, J. J. Xu, X. H. Xia and H. Y. Chen, *J. Am. Chem. Soc.*, 2017, 139, 15479–15485.
- 41 M. Wang, L. Árnadóttir, Z. J. Xu and Z. Feng, *Nano-Micro Lett.*, 2019, **11**, 47.
- 42 M. Wang, B. Han, J. Deng, Y. Jiang, M. Zhou, M. Lucero, Y. Wang, Y. Chen, Z. Yang, A. T. N'Diaye, Q. Wang, Z. J. Xu and Z. Feng, ACS Appl. Mater. Interfaces, 2019, 11, 5682–5686.
- 43 Z. Feng, Q. Ma, J. Lu, H. Feng, J. W. Elam, P. C. Stair and M. J. Bedzyk, *RSC Adv.*, 2015, 5, 103834–103840.
- 44 J. X. Feng, S. Y. Tong, Y. X. Tong and G. R. Li, *J. Am. Chem. Soc.*, 2018, **140**, 5118–5126.
- 45 Y. Cheng, S. Lu, F. Liao, L. Liu, Y. Li and M. Shao, *Adv. Funct. Mater.*, 2017, 27, 1700359.
- 46 J. X. Feng, H. Xu, Y. T. Dong, X. F. Lu, Y. X. Tong and G. R. Li, *Angew. Chem., Int. Ed.*, 2017, **56**, 2960–2964.
- 47 T. Liu, P. Li, N. Yao, G. Cheng, S. Chen, W. Luo and Y. Yin, *Angew. Chem., Int. Ed.*, 2019, **58**, 4679–4684.
- 48 C. L. Green and A. Kucernak, *J. Phys. Chem. B*, 2002, **106**, 1036–1047.
- 49 X. Yang, A.-Y. Lu, Y. Zhu, M. N. Hedhili, S. Min, K.-W. Huang, Y. Han and L.-J. Li, *Nano Energy*, 2015, 15, 634-641.
- 50 D. Voiry, H. Yamaguchi, J. Li, R. Silva, D. C. Alves, T. Fujita, M. Chen, T. Asefa, V. B. Shenoy and G. Eda, *Nat. Mater.*, 2013, 12, 850–855.
- 51 K. Jiang, B. Liu, M. Luo, S. Ning, M. Peng, Y. Zhao, Y. R. Lu, T. S. Chan, F. M. F. de Groot and Y. Tan, *Nat. Commun.*, 2019, 10, 1743.
- 52 A. Damian and S. Omanovic, *J. Power Sources*, 2006, **158**, 464–476.